Novel Core–Shell Polyamine Phosphate Nanoparticles Self-Assembled from PEGylated Poly(allylamine hydrochloride) with Low Toxicity and Increased In Vivo Circulation Time

WILEY-VCH

Novel Core Shell Polyamine Phosphate Nanoparticles Self-Assembled from PEGylated Poly(allylamine hydrochloride) with Low Toxicity and Increased *in vivo* Circulation Time.

*P. Andreozzi, C. Simó, P. Moretti, J. Martinez Porcel, T. U. Luedtke, M. A. Ramirez, L. Tamberi, M. Marradi, H. Amenitsch, J. Llop, M. G. Ortore, S. E. Moya**

Dr. P. A. Author 1, M. S. 2, Dr. J. M. P. Author 4, T. U. L. Author 5, M. A. R. Author 6, L. T. Author 7 and Dr. S. E. M Author 12
Soft Matter Nanotechnology Group, CIC biomaGUNE, Basque Research and Technology Alliance (BRTA), Paseo Miramón 182, 20014 San Sebastián, Guipúzcoa, Spain

Dr. P.A. Author 1
Consorzio Sistemi a Grande Interfase, Department of Chemistry 'Ugo Schiff', University of Florence, Via della Lastruccia 3, 50019 Sesto Fiorentino, FI, Italy.

M. A. R. Author 6
Instituto de Nanosistemas, UNSAM, CONICET, Avenida 25 de Mayo 1021, 1650 San Martín, Buenos Aires, Argentina.

M. S. Author 2, and Dr. J. L. Author 10
Radiochemistry and Nuclear Imaging Group, CIC biomaGUNE, Basque Research and Technology Alliance (BRTA), Paseo Miramón 182, 20014 San Sebastián, Guipúzcoa, Spain

Dr. J. L. Author 10
Centro de Investigación Biomédica en Red – Enfermedades Respiratorias (CIBERES), Av. Monforte de Lemos, 3-5, 28029 Madrid, Spain.

Dr. P. M. Author 3, Dr. M. G. O Author 11
Dipartimento di Scienze della Vita e dell'Ambiente, Università Politecnica delle Marche, Via brecce bianche, I-60131, Ancona, Italy.

Dr. M. M. Author 8
Department of Chemistry 'Ugo Schiff', University of Florence, Via della Lastruccia 3/13, 50019 Sesto Fiorentino, FI, Italy.

Dr. H. A. Author 9
Institute of Inorganic Chemistry, Graz University of Technology, Stremayergasse 9/V, Graz, Austria.

E-mail: smoya@cicbiomagune.es

Keywords: polyamines, polyethylene glycol, ~~self-assembly,~~ core-shell self assembled nanoparticles, ~~antifouling~~toxicity, biodistribution

ABSTRACT

An approach is presented here for reducing toxicity and enhancing therapeutic potential of supramolecular polyamine phosphate nanoparticles (PANs) through PEGylation of polyamines before their assembly into nanoparticles. It is shown that the number of polyethylene glycol (PEG) chains for polyamine largely influence physico-chemical properties of PANs and biological endpoints. Poly(allylamine hydrochloride) (PAH) are functionalized through carbodiimide chemistry with three ratios of PEG molecules per PAH chain: 0.1, 1 and 10. PEGylated PAH is then assembled into PANs by exposing the polymer to phosphate buffer solution. PANs decrease size and surface charge with increasing PEG ratios as evidenced by Dynamic Light Scattering and zeta potential measurements, with the -10 PEG/PAH ratio PANs ~~have~~ having practically zero charge. Small-Angle X-Ray Scattering (SAXS) proves that PEG chains form a shell around a polyamine core, which is responsible for the screening of positive charges. MTT experiments shows as well that the screening of amine groups decrease nanoparticle toxicity, being more evident for the 10 PEG/PAH ratio. Fluorescence Correlation Spectroscopy (FCS) ~~showed~~ proved less interaction with proteins for PEGylated PANs. Positron Emission tomography (PET) in combination with Computed tomography (CT) using ^{18}F labelled PAH PEGylated PANs. Positron Emission tomography (PET) in combination with Computed tomography (CT) using ^{18}F labelled PAH showed longer circulation time in healthy mice for PEGylated PANs than non-PEGylated ones.

1. Introduction

Polyamine phosphate nanoparticles (PANs) are supramolecular assemblies of poly(allylamine hydrochloride) (PAH) and phosphate ions, [1-5] which display a fascinating response to variations in pH. PANs [6] are stable at neutral and moderately basic pH values, from 7 to 9. Outside of this narrow pH range, PANs disassociate into their molecular components. This pH-responsiveness makes PANs a very appealing vehicle for intracellular drug delivery, as they

are stable in physiological media and pH values, but disassemble inside endosomes, i.e. at pH below 6, liberating encapsulated cargo. [7] Besides, the amine groups in the polyamines can protonate inside endosomes, inducing an osmotic swelling that facilitates PANs translocation into cytosol. In a recent paper, ~~some of us~~we have explored the use of PANs prepared with PAH for the delivery of siRNAs and have shown that PANs are capable of successfully silencing green fluorescent protein (GFP) expression at non-toxic concentrations. [6] An increase in PANs concentration however, which could be expected to lead to a more effective silencing, resulted in moderate toxicity, thereby limiting therapeutic use.

PAH toxicity is associated with the presence of primary amines. [8-10] Reducing the toxicity of PANs should increase their potential for drug delivery and facilitate their medical translation. A common procedure to increase biocompatibility of nanoparticles is the use of coatings based on antifouling molecules such as polyethylene glycol (PEG) that is highly hydrated but uncharged and display limited interaction with biomolecules and cells. [11-13] PEG coatings have been extensively used to prolong circulation time of nanoparticles and for generating anti-fouling surfaces. The modification of inorganic nanoparticles with PEG molecules is ~~often~~ frequently performed post synthesis, which often results in limited control of the density of the PEG chains around the nanoparticles. [14] On the other hand, for polymeric nanoparticles or micelles PEG is ~~often~~ in most cases linked to another polymer, as a copolymer or to surfactants before nanoparticle or micelle formation, respectively. [15, 16] PEG density [17] is determinant on the interaction with proteins, and for screening against positive charges. [18] A dense PEG coating around nanoparticles prevents the opsonization process from taking place during circulation, limiting recognition by the Mononuclear Phagocyte System (MPS), and prolonging circulation time. This, ultimately, contributes to a sustained and prolonged delivery of ~~a~~ therapeutic drugs and increase the targeting efficacy of nanoparticles to reach specific organs. [19]

Because PANs are formed by polyamines, they display free accessible amines on their surface, which can be easily modified with COOH-functionalized PEG by carbodiimide chemistry. However, PAH can be functionalised with PEG chains prior to nanoparticle formation, too. In this study we chose to follow the second approach, with the aim of gaining control over ~~PEG~~ chains density of PEG on the nanoparticles. Hence, we have modified PAH with PEG chains, and unreacted amine groups were used to form nanoparticles through complexation with phosphates. Interestingly, we observed that PANs retain their ability to disassemble at endosomal pH values, despite the changes in their physico-chemical characteristics ~~with the number of PEG chains attached per PAH molecule~~. While the association of PAH chains trough phosphate was not prevented by PEGylation, we will show by Dynamic Light Scattering (DLS), zeta potential measurements and Small Angle X-ray Spectroscopy (SAXS) that the number of PEG molecules per PAH chain played a fundamental role in the organisation of the polyamines into PANs, leading to a core shell structure with PEG forming a shell around a polyamine core. PEG chains impose steric constrains that affect the size of the PANs and the capacity of association among polymer chains. PEGlylation of PAH affects PANs-protein interactions as observed by Fluorescence Correlation Spectroscopy (FCS) [20] nanoparticle toxicity, and circulation time as determined by Positron Emission Tomography., thus enhancing their potential for drug delivery applications.

2. Results and Discussion

PAH molecules were conjugated with PEG-hydroxysuccimide through amide formation. Synthetic conditions for PEGylation are detailed in the experimental section. After PEGylationof PAH, PANs were formed by addition of PBS to the polymer solutions. PEG chains were attached to PAH molecules with three different ratios of PEG per PAH chain (PEG_x:PAH): $PEG_{0.1}$:PAH, PEG_1:PAH, PEG_{10}:PAH respectively. The PEG_x:PAH ratio was confirmed by NMR (see supporting information, Figure 1). The formation of PANs with

PEGylated PAH was confirmed and characterised by DLS, Transmission Electron Microscopy (TEM), zeta potential measurements, and SAXS studies. DLS shows that the size of the PANs decreases as the number of PEG chains per PAH chain increases, for the same PBS concentration and ionic strength (**Figure 1**). In the case of $PEG_{0.1}$:PAH, the hydrodynamic diameter of the PEGlyated PANs is the same as for PANs formed by PAH (non-PEGylated), approximately 125 nm, and decreases to about half for PEG_1:PAH and to about 25 nm for PEG_{10}:PAH. TEM PEGylated PANs display a well-defined spherical shape and an average diameter of around 25 nm (Figure 1). Both TEM and DLS evidence that PEGylation does not prevent PAN formation, although it has a clear influence on particle size. Additionally, PEGylation does not prevent the characteristic response of PANs with pH. DLS data show that PEGylated PANs disassemble at pHs around 5, where counts are practically 0 (supporting information Figure 2).

The attachment of uncharged PEG chains also has an impact on particle charge. ζ-potential measurements show a decrease in the ζ-potential of PANs as the number of PEG chains per PAH increases, from +20 mV for the unmodified PANs to less than +5 mV for both PEG_1:PAH and PEG_{10}:PAH (**Figure 2**). ζ-potential values for PEG_x:PAH below +5 mV can actually be considered 0, meaning that the charged from PAH are completely, or almost completely, screened by the PEG chains. The formation of a PEG shell around the PANs that screens the positive charges from PAH would explain the decrease in ζ-potential with PEGylation as well as the decrease in the size of the PANs as the number of PEG chains per PAH molecule increases. This is likely due to the arrangement of the PEG chains limiting the interaction of non-PEGylated segments of PAH and imposing steric constrains for nanoparticle formation and growth.

SAXS measurements were conducted precisely to prove the hypothesis of a core-shell structure for the PEGylated PANs. SAXS provides information regarding average dimensions of the particles in solution and their structural features. While DLS results determine the number

density of spherical nanoparticles and their size distribution around an average value, SAXS is capable of distinguishing polymers with different electron densities, hence, it can be used to prove a different spatial organisation of PAH and PEG inside the nanoparticle.

SAXS measurements were performed with PANs prepared with the three PEG_x:PAH ratios and with different phosphate buffer concentrations and ionic strengths. The experimental set up of the SAXS allows us to accurately determine the size of PANs and their PEGylated shell, considering fixed values of the electron density of both polymers in all the experimental conditions as taken from literature. [21, 22] Experimental data can be then very well fitted assuming a core shell structure with a core with the electronic density of PAH and the shell with that of PEG (**Figure 3**). From SAXS data analysis, a clear trend in nanoparticle size as a function of PEG_x:PAH is observed. In fact, as the PEG_x:PAH ratio increases, PAN`s dimensions decrease, in agreement with DLS results (Figure 3, right panel). For the smallest PEG_x:PAH ratio, 0.1, PANs size varies with the concentration of phosphate buffer. We observed variations in size of about a 30% when going from 2 to 10 mM PBS but when the ratio is 1, size of PANs becomes less dependent on buffer concentration (confirmed by DLS, data not shown). For PEG_{10}:PAH, the size remains almost constant with, PBS concentration. As the number of PEG chains per PAH molecule increases the number of chains of PAH that can be associated in the PANs must decrease to cope with the constrain of arranging PEG chains on the surface of the PANs. The arrangement of PEG chains makes it difficult for the PANs to increase size with increasing PBS concentration. An increase in PBS concentration allows for more PAH chains to associate in a non-PEGylated PAN triggering particle grow. For the $PEG_{0.1}$:PAH ratio, since there is one PEG chain every 10 PAH chains we observe that PBS concentration still influences particle growth. PEG chains are easy to accommodate in the surface of the PAN in these conditions. We must think in discrete PEG chains, not forming a complete coating and the addition of one PEG chain to the nanoparticle would allow for an increase in 10 chains of PAH per particle. As the number of PEG chains increase per PAH chain more PEG have to be

accommodated on the surface of the PANs and this difficult additional growth of the PANs with PBS. This is particularly evident for 10 PEG chains per PAH. One additional chain of polymer in the PAN would imply 10 additional PEG chains to be located on the surface of the nanoparticles. Besides, there is the additional difficulty for the association of non-PEGylated segments of the polymer while arranging the PEG chains on the surface. For the ionic strength we can make similar considerations. Increasing ionic strength results in more coiled conformations for the polyamines and in less electrostatic repulsion among them, which favours larger particle. Ionic strength should have less impact on conformation of PEGylated PAH chains as the PEG side chains are not charged. Therefore, the steric constrains imposed by the PEG chains should not be affected by the ionic strength~~, which~~. The ~~becomes more relevant the~~ larger the number of PEG chain per PAH molecule ~~is~~the weaker the influence of the ionic strength becomes.

T~~he t~~hickness of the PEG shell obtained from SAXS data has been plotted as a function of the PEG_x:PAH ratio and PBS concentration (**Figure 4**). ~~We can observe from the data that increasing~~ Increasing the number of PEG chains per PAH molecule results in a decrease in thickness of the PEG shell. The thinnest PEG shells are observed for PEG_{10}:PAH. For this number of PEG chains, ζ-potential results suggested the presence of a denser PEG shell. Taking together DLS and SAXS results, it is possible to understand the decrease in thickness with increasing number of PEG chains considering that the steric constraint of PEG_{10}:PAH leads to a smaller association of PAH chains, and in this situation the total number of PEG chains on the surface of the nanoparticle may be lower than at 0.1 and 1 PEG_x:PAH ratios, resulting in a smaller thickness of the PEG shell. However, since the size of the PAH core is also small for the PEG_{10}:PAH ratio, the screening of the charged core is more effective. PEGylation of PAH did not prevent the polyamines from assembling while at the same time succeed in screening positive charges from amines. The screening of positive charges can have an impact on toxicological endpoints of the PANs and in their biological fate.

In order to assess toxicity after PEGylation, an MTT assay was conducted for two immortalized cell lines, Hela and 4T1, at three time points corresponding to 3, 24 and 48 hours (**Figure 5**). HeLa cells are less affected than 4T1 cells in their proliferation by PANs. In case of HELA cells, control nanoparticles, unmodified PANs, and PANs with a $PEG_{0.1}$:PAH ratio have not a significant impact on proliferation up to a concentration of 0.05 mg/mL for every time point considered for this cell line. Above this concentration, proliferation decreases below 50 % for the unmodified PANs and $PEG_{0.1}$:PAH while it remains high for PEG_1:PAH and PEG_{10}:PAH. In the case of PEG_1:PAH, an increase in polymer concentration results in a progressive decrease of proliferation. At 0.1 mg/mL polymer PEG_1:PAH PANs reduce cell proliferation to a 50 % and can be therefore considered toxic. At 0.25 mg/mL PEG_1:PAH PANs, cells show low cell proliferation, comparable with the proliferation in the presence of unmodified PANs and $PEG_{0.1}$:PAH PANs. This behaviour is observed for the three time points considered. For PEG_{10}:PAH PANs, cell proliferation is practically unaffected for all concentrations considered at the three time points.

For 4T1 cells we observe that while at low PAN concentrations, cell proliferation is similar to that of HELA cells, when PAN concentration increases cells become more sensitive to the ~~PANs~~nanoparticles. At 3 hours, all PANs can be considered non-toxic up to 0.025 mg/mL at 0.1 mg/mL proliferation decreases to 50 % for non-PEGylated PANs, $PEG_{0.1}$:PAH, and also for PEG_1:PAH. Overall, we see that the PEG_1:PAH PANs result in a decreased cell proliferation in this cell line compared with the HeLa cell line. At 24 h we observe that the PEG_1:PAH nanoparticles are already toxic at 0.05 mg/mL, with a cell proliferation of less than 40 %. At 48 h cell proliferation is lower than 40 % at 0.025 mg/mL. For PEG_{10}:PAH PANs, cell proliferation is less affected. At 3 h, only at the highest concentration, 0. 25 mg/mL, cell proliferation values approach 50 %, hinting to a toxic effect. After 24 h, 50 % proliferation can be observed for 0.1 mg/mL PANs, and less than a 20% proliferation for 0.25 mg/mL. At 48 h cell proliferation decreases to less than 40 % at 0.1 mg/mL.

Overall, PEGylation of PAH has a positive effect on cell proliferation for PEG_1:PAH and PEG_{10}:PAH ~~PEG_x:PAH ratios 1 and 10~~ when compared with non-PEGylated, or the $PEG_{0.1}$:PAH ratio for same doses of PANs. This effect accounts for the screening of positive charges from the PEG shell around the nanoparticles and agrees with the physico-chemical data, which show negligible zeta potential for the PEG_1:PAH and PEG_{10}:PAH ratios and a screening of the positive charges of the amines. However, it must as well be considered that there is a reduction of the number of charges per mg of polymer when we use PEGylated PAH.

An important aspect of the PEG shell is its capacity to prevent, or decrease, the interaction of proteins with the PANs, which can have large impact on PANs recognition by the immune system, and also in the translocation process at tissue and cell levels. [23] To assess the interaction of PEGylated PANs with proteins, we performed a Fluorescence Correlation Spectroscopy (FCS) study. This technique allows us to trace the diffusion of fluorescent molecules, or objects, by recording fluctuations in fluorescence intensity within a confocal volume. [24, 25] PAH chains were fluorescently labelled with prior to PEGylation. Experiments were performed for non-PEGylated PANS and PEG_{10}:PAH PANs. Fluorescently labelled PEGylated PANs were exposed *in situ* to a concentration of Bovine Serum Albumin (BSA) proteins equal to 800 μM, to simulate physiological conditions. We observe an increase in diffusion time for non-PEGylated and PEG_{10}:PAH PANs in the presence of proteins, **Figure 6**. The increase in diffusion time is associated with the interaction of proteins with the PANs as a result of the formation of a protein corona around the PANs. From the diffusion time, we can obtain the size of the PANs before and after exposure to the proteins, and although size changes for both PAN types, there is a much larger increase in particle diameter for non-PEGylated PANs compared to PEGylated ones. Indeed, the average size of the PANs increases in the presence of BSA for non-PEGylated and PEGylated PANs, respectively (see supporting information Table 1). Here, we ~~PEG_x:PAH~~exposed PANs to proteins and we do not remove excess of proteins from the media. In this situation we expect the formation of a soft protein

corona around the PANs, ~~that means we look~~meaning that we sense with FCS ~~at~~ all proteins interacting with the PANs, not only the strongly bound (hard corona), but also proteins weakly bound, and for this we observe a relatively large increase in size of the particles. It may also mean a certain degree of aggregation; however, this ~~is not observed in~~can not be concluded from the amplitude of the correlation functions. In any case, PEGylated PANs show less association with proteins compared to non-PEGylated ones~~. These experiments show, anyway, that~~, but proteins bind around the PEGylated PANs, which may indicate that there is enough free space between PEG chains to access to ~~the~~ amine groups.

PET-CT studies were conducted in order to investigate the *in vivo* biodistribution of ^{18}F labelled PANs prepared with PAH and PEG_{10}:PAH. Radiolabelling was performed as described in the experimental section through conjugation of a pre-labelled prosthetic group, [^{18}F]F-PyTFP, to free amines in PAH and PEG_{10}:PAH. A radiochemical yield of 50% (with respect to [^{18}F]F-PyTFP, decay-corrected) was achieved after 5 min incubation at room temperature of PAH or PEG_{10}:PAH with [^{18}F]F-PyTFP. Radiochemical purity after purification was ≥99% for both cases, as determined by instant thin layer chromatography. Animals were injected with equal concentrations of either PANs or PEGylated PANs. From PET images (Figure 7A ~~and C~~) the concentration of radioactivity as a function of time per organ was evaluated (Figure 7C). Visual inspection of PET images suggests that the two nanoparticles have ~~show~~ different fates. Whole body reconstruction of PET-CT images (Fig 7b) at 240 min clearly show the different distribution of the PEGylated and non PEGylated PANs in the animal body. At short times after administration, non-PEGylated PANs show higher accumulation in the lungs and the liver than PEGylated PANs, while PEGylated PANs show higher accumulation in the heart during the first 25-30 min. At longer times, activity in the heart is higher for the non-PEGylated PANs, while to a large extent PEGylated PANs tend to accumulate in the bladder. The higher activity in the heart for the PEGylated PANs suggest a higher concentration of the PANs in blood. The progressive increase of radioactivity in the bladder is indicative of the PEGylated PANs being

eliminated by urine. Biodistribution data shows that the PEGylated PANs have a longer circulation time compared to the non-PEGylated PANs and are more easily excreted through urine. These results are in agreement with the expected effect of PEGylation, which increases the circulation of nanoparticles by avoiding clearance by the mononuclear phagocyte system. The higher percentage of PEGylated PANs in the bladder and elimination through urine is likely related to the smaller size of these nanoparticles compared to the non-PEGylated ones.

Conclusions

PEGylation of PAH molecules does not prevent formation of PANs in presence of phosphate buffer but largely affects size and charge of the formed particles. Increasing the number of PEG chains per PAH molecule from 0.1 to 10 results in progressive decrease of the size and zeta potential of the nanoparticles, with zeta potential becoming practically 0 for 10 PEG chains per PAH. At this ratio of PEG to PAH the size of PANs decrease to 10 nm and size is practically not affected by PBS concentration. This decrease in size can be understood as a result of the topological constrains to accommodate the PEG chains while free amino groups from different polymer chains associate through interaction with phosphates.

PANs with 10 PEG molecules per PAH chain display a core shell structure with PEG chains forming the external shell as shown by SAXS measurements. The organization of PEG chains as a shell around a polyamine core is responsible of shielding positive charges from PAH as observed by zeta potential measurements and results in a decrease particle toxicity. PEGylation of PANs reduces interactions as well with proteins and prolong PANs circulation in vivo. Overall, we have shown here that by PEGylating PAH PANs characteristics are largely changed, with a shielding of positive charges in PANs as result of the presence of PEG as external shell enhancing PANs potential for biomedical applications by decreasing toxicity and extending nanoparticle circulation

4.Experimental Section

Materials. Poly(allylamine hydrochloride) salt (PAH) (MW: 15 x 10^4 g/mol), Phosphate Buffer Salt tablets (PBS), Sodium Phosphate dibasic (Na_2HPO_4), Potassium Phosphate monobasic (KH_2PO_4), Hydrochloric Acid (HCl), Sodium Hydroxide (NaOH) and Sodium Chloride (NaCl), NHS-PEG-OH (5000 Da), all from Sigma-Aldrich, were used as received. Polyelectrolyte stock solutions and all subsequent diluted precursor solutions were prepared with MilliQ deionized water. Human lung adenocarcinoma (A549 CCL-185), breast cancer (4T1), HeLa cell lines were purchased from the American Type Culture Collection (ATCC, USA). RPMI and DMEM medium were purchased from Lonza (USA). 3,4,5-dimethylthiazol-2,5 biphenyl tetrazolium bromide (MTT), Penicillin-streptomycin, were purchased from Sigma Aldrich (USA). Grids and supports of copper and ammonium molybdate were obtained from Electron Microscopy Sciences (USA).

Synthesis of PEGylated Polyamine (PEG_x-PAH). **Synthesis of PEGylated Polyamine (PEG_x:PAH).** PAH was modified with PEG chains at different PEG_x:PAH molar ratios:0.1, 1 and 10 PEG molecule per polyamine chain. In brief, 40 µL of 500 mg/mL PAH stock solution were added to 50 mL falcon tubes containing 18.4 mL, 18 mL, and 13.5 mL of MilliQ H_2O (for samples with molar ratios 0.1, 1 and 10, respectively), to a final PAH concentration of 1 mg/mL (6.7 x 10^{-5} M, 15000 MW). The pH of the solution was adjusted to 8 by dropwise addition of 1.5 mL of 0.1 M NaOH solution~~()~~, to trigger the reaction between the *N*-hydroxysuccinimide esters present on the PEG chains and the amine groups of PAH. Finally, we added 50 µL, 500 µL or 5000 µL of 13.30 mg/mL PEG (2.66 mM, 5000 MW) in DMSO stock solution to obtain a final volume of 20 mL and a PEG concentration of 0.0332 mg/mL, 0.332 mg/mL and 3.32 mg/mL, respectively. Reactions were carried out at room temperature and then placed at 4 °C for 4 h under stirring. Solutions were dialyzed against 100 mL of MilliQ H_2O using a dialysis

cassette with a molecular weight cut-off of 10 KDa to remove the excess of PEG (dialysis water was exchanged three times, after 30 min, 90 min and over-night dialysis). The dyalized solutions were lyophilized for 48 h resulting in white cotton like powders, stored afterwards at -20 °C.

Dynamic Light Scattering (DLS). Dynamic Light Scattering measurements were carried out with a Malvern ζ-Sizer Instrument in backscattering mode. All studies were performed at a 173° scattering angle, temperature controlled at 25 °C in 1 mL polystyrene cuvettes. PANs were characterised in terms of size and ζ-potential. Short time measurements were carried out over 15 min, with 3 consecutive measurements for each sample. ζ-potential measurements were performed in auto-mode at 25 °C, with 3 consecutive measurements per sample.

Transmission Electron Microscopy (TEM). For transmission electron microscopy analysis of PEGylated PANs, normal and ultra-thin carbon film coated grids were used. 2 μL of undiluted PEG_{10}:PAH with concentration of 2 mg/mL (assembled 30 min prior to grid deposition of samples) were transferred to plasma coated grids and incubated for 1 min, followed by washing with degassed Nanopure water, incubation with 3 μL of ammonium molybdate 20 mg/mL for 1 min, and three final washes with degassed Nanopure water. Transmission electron microscopy analysis was performed by using a JEOL JEM 1010 microscope operating at an acceleration voltage of 120 kV.

Small Angle X-Ray Scattering (SAXS). Small Angle X-ray Scattering (SAXS) experiments were performed at the Austrian SAXS beamline in Elettra Synchrotron, Trieste, Italy. [26] i Measurements were carried out at 20 °C in an auto-sampler developed in the beamline: the μ-Drop sample changer μDrop: a system for high-throughput SAXS measurements of microlitre samples. [27] The μ-Drop system has several advantages over a capillary based setup, the most important being that because just a single drop is placed, the used volume is 15 μL in a

capillaries of 1.5 mm outer diameter/0.01 mm wall thickness made from borosilicate (Hilgenberg, Maisfeld, Germany), enclosed within a thermostatic compartment connected to an external circulation bath and a thermal probe for temperature control. A Pilatus3 1 M detector system based on the CMOS hybrid pixel technology recorded the bidimensional patterns, stored in TIF format and then processed with FIT2D [28] and Igor Pro (WaveMetrics, Lake Oswego, OR, USA) software. In detail, the incident and transmitted intensities were measured, data were corrected for sample transmission and fluctuations of the primary beam, each scattering patterns from all images of each sample were averaged and the respective backgrounds, treated in the same way, were subtracted. Scattering patterns were converted to absolute intensity by rescaling the forward intensity with BSA solution (5.0 mg/mL in phosphate buffer) and water scattering. 2D detector images were radially averaged to obtain the scattering intensity as a function of the magnitude of the scattering vector Q defined as $Q = 4\pi \sin\theta/\lambda$, with 2θ being the scattering angle and λ equal to 0.154 nm the X-ray wavelength (corresponding to an energy of 8 keV). We measured at least three different volumes of the same sample and at least 4 times each volume, with an acquisition time of 20 s and a rest time of 3 s for each step. According to this procedure we aim to reduce the possibility to induce radiation damage. Raw data were radially averaged and calibrated in absolute units (cm^{-1}) by using a freshly prepared BSA solution (5.0 mg/mL) in phosphate buffer and water. The sample-to-detector distance was set to 1.247 m, which provided wavenumbers Q by the equation $Q = 4\pi \sin\theta/\lambda$, with 2θ being the scattering angle and λ equal to 1.54 Å the X-ray wavelength. Both polymers solutions (at concentration c = 1.0 mg/mL) and buffers were measured at the same conditions concerning temperature and exposure time. SAXS data analysis is based on a core-shell model, according to equation 1:

$$\frac{d\Sigma}{d\Omega} = n_{NP}\left\{\frac{4}{3}\pi\left[(\rho_{PEG}-\rho_0)(R+\delta)^3\phi\big(Q(R+\delta)\big)+(\rho_{PANS}-\rho_{PEG})R^3\phi(QR)\right]\right\}^2 \quad (1)$$

with $\phi(x) = 3\frac{\sin x - x\cos x}{x^3}$. n_{NP} is the nanoparticle number density, ρ_{PEG}, ρ_0, and ρ_{PANS} are the outer shell, the bulk, and the PANs electron densities, respectively, R is the PAN average radius, and δ is the external shell thickness. The average radius of PANs has been considered polydisperse, in agreement with DLS results, according to GENFIT software procedures, [29] the software used to fit our experimental SAXS data.

Fluorescence Correlation Spectroscopy (FCS). Green Rhodamine labelled PAH (G-PAH) and green Rhodamine labelled PEG_{10}:PAH ~~was~~ were dissolved in MilliQ H_2O to a final concentration of 10 mg/mL of. 3 µL of this stock solution were diluted in 270 µL of 5 mM PBS, in order to allow nanoparticle formation, non PEGylated and PEGylated PANs respectively. ~~The nanoparticles~~ PAH labeled with green rhodamine (G-PAH) was provided by Surflay AC, Germany. Green labelled PEG_{10}:PAH was prepared by PEGylation of G-PAH with 10 PEG chains as described for the non labelled PAH. ~~The nanoparticles~~Nanoparticles were then suspended in a solution with BSA in Milli-Q H_2O to study the formation of the shell protein. The final concentration of BSA was 800 µM. ~~The nanoparticles~~Nanoparticles were kept for 1 h at 37 °C under stirring at 200 rpm. FCS measurements were performed with the LSM510 confocal microscope from Zeiss and data acquisition was performed with Zen black software. The laser source was a DPSS 561-10 laser with a wavelength of 561 nm and a 40 C Apo/1.2 W DICIII with water immersion objective. The confocal volume was calibrated with Rhodamine B (50 nM) and its known diffusion coefficient of 4.50 x 10^{-6} cm^2s^{-1}. [30] Each measurement consisted of at least 10 runs each one of 10 seconds. FCS data evaluation was done with the open-source software QuickFit. Autocorrelation functions were fitted with a 2 components 3D diffusion model and by using the fit algorithm *Simulated Annealing* and *Levenberg-Marquardt.* [31]

Cell Culture. Human lung adenocarcinoma (A549) and breast cancer (4T1) cell lines were cultured with RPMI 1640 medium supplemented with 10 % (v:v) fetal bovine serum (FBS) and 1 % (v:v) antibiotic solution (100 units/mL penicillin, 100 mg/mL streptomycin, P/S). Cells were maintained at 37 °C, 5 % CO_2 in a humidified chamber. Cervical cancer cell lines (HeLa) were cultured with DMEM medium supplemented with 10 % of FBS, 1 % P/S.

Cell Viability MTT Assay. Cell mitochondrial activity was tested using the 3-(4,5-dimethylthiazol-2-yl)-2,5-diphenyl tetrazolium bromide (MTT) assay, which is based on the mitochondrial conversion of the tetrazolium salt into a formazan dye with absorption characteristics in the visible region. PANs were incubated with cells at different concentrations and different time points (3 – 48 hours). Following incubation with PEGylated PANs at each time point, cells were washed and 135 µL fresh medium with 15 µL of MTT (at 5 mg/mL in PBS) were added to each well. Non-functionalised PAH was used as a control. Culture plates were then incubated at 37 °C. After 2 hours incubation, medium-containing MTT was discarded and formazan crystals were dissolved in 150 µL DMSO. The absorbance at 550 nm (with automatic discount of ref wavelength 630 nm) of the resulting solution was measured in a 96-well spectrophotometer microplate reader. Percentage cell mitochondrial activity was determined by the following formula: (Absorbance of treated cells/ Absorbance of control cells) x 100%.

Synthesis of 6-[^{18}F] Fluoronicotinic Acid 2,3,5,6-Tetrafluorophenyl Ester ([^{18}F]F-PyTFP). [^{18}F]fluorine was produced in a cyclotron (18/9 MeV Cyclone, IBA, Belgium) by proton irradiation of an ^{18}O-enriched water target via the ^{18}O(p, n)^{18}F nuclear reaction. [^{18}F]F-PyTFP was synthesised using a TRACERlab FX-FN synthesis module (GE Healthcare), following a previously reported method. In brief, aqueous [^{18}F] fluoride was first trapped in an ion-exchange resin (Sep-Pak® Accell Plus QMA Light) and subsequently eluted to the reactor vessel with a solution of Kryptofix $K_{2.2.2}/K_2CO_3$ in a mixture of water and acetonitrile. After

azeotropic drying of the solvent, a solution of F-PyTFP (10 mg) in a mixture of tert-butanol and acetonitrile (4/1) was added and the mixture heated to 40 °C for 15 min. The reaction mixture was then diluted with 1 mL of acetonitrile and 1 mL of water, and purified by HPLC using a Nucleosil 100-7 C18 column (Machery-Nagel, Düren, Germany) as the stationary phase and 0.1% TFA/acetonitrile (25/75) as the mobile phase at a flow rate of 3 mL/min. The desired fraction (22-23 min [^{18}F]F-PyTFP) was collected, diluted with water (25 mL), and flushed through a C18 cartridge (Sep-Pak® Light, Waters) to selectively retain [^{18}F]F-PyTFP. The desired labelled specie was finally eluted with acetonitrile (1 mL). Radiochemical purity was determined by radio-HPLC using a Mediterranean C18 column (4.6 x 150 mm, 5 µm) as the stationary phase and 0.1% TFA/acetonitrile (0-1 min 25% acetonitrile; 9-12 min 90% acetonitrile; 13-15 min 25% acetonitrile) as the mobile phase at a flow rate of 1.5 mL/min (retention time: 8 min).

Radiolabelling and formation of PANs with [^{18}F]F-PyTFP. The radiofluorination of PANs was carried out by the reaction between the free amine groups from PAH and [^{18}F]F-PyTFP. In brief, 200 µL of PAH in 1 M TRIS buffer pH 8 (1 mg/mL) and 5 µL of [^{18}F]F-PyTFP in acetonitrile (140 ± 10 MBq) were mixed and incubated at room temperature for 5 min. After incubation, the reaction mixture was purified by size exclusion chromatography using Illustra™ Nap™-5 Sephadex™ columns G-25 DNA grade (GE Healthcare, USA), preconditioned in 5 mM PBS buffer pH 7.4. The fractions containing pure labelled compound were collected, measured in a dose calibrator and determined by radio-thin layer chromatography (radio-TLC) using iTLC-SG chromatography paper (Agilent Technologies, CA, USA) and dichloromethane and methanol (2/1) as the stationary and mobile phases, respectively. TLC plates were analysed using TLC-reader (MiniGITA, Raytest). ^{18}F-labelled PANs were synthetised during the purification step (1 mg/mL PAH in 5 mM PBS). The same methodology described above was

followed for the radiolabelling and formation of PANs with the PEG modification. Instead of 5 mM PBS, 10 mM PBS pH 7.4 was used for the formation of the nanoparticles.

Animals. Female mice (BALB/cJRj, 10 weeks, Janvier; 6 animals) weighing 22 ± 2 g were used to conduct the biodistribution studies. The animals were maintained and handled in accordance with the Guidelines for Accommodation and Care of Animals (European Convention for the Protection of Vertebrate Animals Used for Experimental and Other Scientific Purposes) and internal guidelines. All experimental procedures were approved by the ethical committee and the local authorities before conducting experimental work (Code: PRO-AE-SS-059).

In vivo biodistribution studies in mice. Animals were anesthetised by inhalation of 3% isoflurane in pure O_2 and maintained by 1.5-2% isofluorane in 100% O_2. ^{18}F-PANs/-PANs-PEG were administered intravenously (2.7 ± 0.4 MBq, 110 µL, 22 ± 2 µg of NP, injected via one of the lateral tails veins) using 5- or 10-mM PBS pH 7.4 as a vehicle (n=3 per NP type). Dynamic, whole body 30-min PET scans were started immediately after administration of the labelled compound and static 10-min PET scans were performed at t= 2 and 4 hours after administration using the MOLECUBES β-CUBE (PET) scanner. After each PET scan, whole body, high resolution CT acquisitions were performed on the MOLECUBES X-CUBE (CT) scanner to provide anatomical information of each animal as well as the attenuation map for later image reconstruction. Random and scatter corrections were automatically applied during image reconstruction (3D OSEM reconstruction algorithm). PET-CT images of the same mouse were co-registered and analysed using the PMOD image processing tool. Volumes of interest (VOIs) were manually delineated on selected organs (brain, lungs, liver, stomach, kidneys, spleen, and bladder). To obtain an estimation of the concentration of radioactivity in the blood, a VOI was drawn on the heart. Time–activity curves (decay corrected) were obtained as cps/cm^3 in each organ. Curves were transformed into real activity (Bq/cm^3) curves by using a calibration factor, obtained from previous scans performed on a phantom (micro-deluxe, Data spectrum Corp.)

under the same experimental conditions (isotope, reconstruction algorithm and energetic window. 3D images were obtained by a 3D image analysis cloud service developed by Multimodal 3D L.L.C. [32]

Supporting Information
Supporting Information is available from the Wiley Online Library or from the author.

Acknowledgements
~~Acknowledgements~~

The authors thank Elettra Synchrotron for beamtime allocation. The authors thank as well the Central European Research Infrastructure Consortium (CERIC) for travel support, and Barbara Sartori for her technical assistance in the chemical laboratory. We thank Multimodal 3D for 3D image analysis. We also thank Dr. Richard Murry for correcting the manuscript. S. E. Moya and J. Llop thank the MAT2017-88752-R and CTQ2017-87637-R Retos projects, respectively, from the Ministerio de Economía, Industria y Competitividad, gobierno de España. This work was performed under the Maria de Maeztu Units of Excellence Program from the Spanish State Research Agency – Grant No. MDM-2017-0720.

Author Contributions

ha formattato: Tipo di carattere: Grassetto, Non Corsivo

P.A. and S.E.M.- conceived and designed the study. J.M.P and M.A.R. synthesized and characterized by TEM PEGylated PANS. C.S. performed radioactive labelling andPET/CT scans and data analysis. P.A. did DLS experiments. L.T. did cell viability studies. T.L. measured FCS. H.A., P.A., M.G.O and S.E.M. conducted SAXS experiments. P.M. and M.G.O. analyzed SAXS data. P.A., M.M., M.G.O., S.E.M., and J.L. analyzed and discussed the data. P.A. and S.E.M. have written this manuscript. All authors have read and approved the final manuscript.

((Acknowledgements, general annotations, funding. Other references to the title/authors can also appear here, such as "Author 1 and Author 2 contributed equally to this work."))

Received: ((will be filled in by the editorial staff))
Revised: ((will be filled in by the editorial staff))
Published online: ((will be filled in by the editorial staff))

References

ha formattato: Tipo di carattere: Grassetto

[1] W. A. Marmisollé, J. Irigoyen, D. Gregurec, S. Moya, O. Azzaroni, *Adv. Funct. Mater*. **2015**, *25*, 4144.

[2] V. S. Murthy, R. R. Rana, M. S. Wong, *J. Phys. Chem.* B **2006**, 110, 25619.

[3] K. Lutz, C. Gröger, M. Sumper, E. Brunner, *Phys. Chem. Chem. Phys.* **2005**, 7, 2812.

[4] M. L. Agazzi, S. E. Herrera, M. L. Cortez, W. A. Marmisollé, M. Tagliazucchi, O. Azzaroni, *Chem.–Eur. J.* **2020**, 26, 2456.

[5] S. E. Herrera, M. L. Agazzi, M. L. Cortez, W. A. Marmisollé, M. Tagliazucchi, O. Azzaroni, *Chem. Phys. Chem.* **2019,** 20 (8) , 1044-1053.

[6] P. Andreozzi, E. Diamanti, K. R. Py-Daniel, P. R. Cáceres-Vélez, C. Martinelli, N. Politakos, A. Escobar, M. Muzi-Falconi, R. Azevedo, S. E. Moya, *ACS Appl. Mater. Interfaces*, **2017**, 9, 38242.

[7] D. Di Silvio, M. Martínez-Moro, C. Salvador, M. de los Angeles Ramirez, P. R. Cáceres-Vélez, M. G. Ortore, D. Dupin, P. Andreozzi, S. E. Moya, *J. Colloid Interface Sci.*, **2019**, 557, 757.

[8] A. E. Pegg, *Chem. Res. Toxicol.* **2013**, 26, 1782.

[9] O. Boussif, T. Delair, C. Brua, L. Veron, A. Pavirani, H. V. J. Kolbe, *Bioconjug. Chem.* **1999**, 10, 883.

[10] J. H. Yu, J. Huang, H. L. Jiang, J. S. Quan, M. H. Cho, C. S Cho, *J. Appl. Polym. Sci.* **2009**, 112, 933.

[11] S. Lowe, N. M. O'Brien-Simpson, L. A. Connal, *Polym. Chem.* **2015**, 6, 198.

[12] H. Otsuka, Y. Nagasaki, K. Kataoka, *Adv. Drug Deliv. Rev.* **2003**, 55, 403.

[13] L. E. van Vlerken, T. K. Vyas, M. M. Amiji, Pharmaceutical Research, **2007**, 24, 1405.

[14] J. Kučka, H. Macková, V. Lobaz, P. Francová, V. Herynek, T. Heizer, P. Páral, L. Šefc, *Sci. Rep.* **2019**, 9, 10765.

[15] W. Celentano, J. Battistella, I. Proietti Silvestri, R. Bruni, X. Huang, M. Li, P. Messa, S. Ordanini, F. Cellesi, *React. Funct. Polym.* **2018**, 131, 164.

[16] K. K. Gill, A. Kaddoumi, S. Nazzal, *J. Drug Target* **2014**, 23, 222.

[17] K. Knop, R. Hoogenboom, D. Fischer, U. S. Schubert, *Angew. Chem. Int. Ed.* **2010**,49, 6288.

Katrin Knop, Richard Hoogenboom, Dagmar Fischer, and Ulrich S. Schubert

[18] R. Michel, S. Pasche, M. Textor, D. G. Castner, *Langmuir* **2005**, 21, 12327.

[19] R. Gref, Y. Minamitake, M. T. Peracchia, V. Trubetskoy, V. Torchilin, R. Langer, Science **1994**, 263, 1600.

[20] C. Röcker, M. Pötzl, F. Zhang, W. J. Parak, G. U. Nienhaus, *Nat. Nanotechnol.* **2009**, 4, 57.

[21] P. Andreozzi, C. Ricci, J. E. M. Porcel, P. Moretti, D. Di Silvio, H. Amenitsch, M. G. Ortore, S. E. Moya, *J. Colloid Interface Sci.* **2019**, 543, 335.

[22] M. Maccarini,G. Briganti, S. Rucareanu, X. Lui, R. Sinibaldi, M. Sztucki, B. Lennox, *J. Phys. Chem. C* **2010**, 114, 6937.

[23] M. P. Monopoli, C. Åberg, A. Salvati, K. A. Dawson, *Nat. Nanotechnol.* **2012**, 7, 779.

[24] S. Jazani, I. Sgouralis, O. M. Shafraz, M. Levitus, S. Sivasankar, S. Pressé, *Nat. Commun.* **2019**, 10, 3662.

[25] E. L. Elson, *Biophysical Journal*, **2011**, 101, 2855.

[26] H. Amenitsch, M. Rappolt, M. Kriechbaum, H. Mio, P. Laggner, S. Bernstorff, *J. Synchrotron Radiat.* **1998**, 5, 506.

[27] R. Haider, B. Sartori, A. Radeticchio, M. Wolf, S. Dal Zilio, B. Marmiroli, H. Amenitsch, *J. Appl. Cryst.* **2021**, 54, 132.

[28] A. P. Hammersley, K. Brown, W. Burmeister, L. Claustre, A. Gonzalez, S. McSweeney, E. Mitchell, J. P. Moy, S.O. Svensson, A. W. Thompson, *J. Synchrotron Radiat.* **1997**, 4, 67.

[29] F. Spinozzi, C. Ferrero, M. G. Ortore, A. De Maria Antolinos, P. Mariani, *J. Appl. Crystallogr.*, **2014**, 47, 1132.

[30] P.O. Gendron, F. Avaltroni, K. J. Wilkinson, *J. Fluoresc.* **2008**, 18, 1093.

[31] A. Silvestri, D. Di Silvio, I. Llarena, R. A. Murray, M. Marelli, L. Lay, L. Polito, S. E. Moya, *Nanoscale*, **2017**, 9, 14730.

[32] R. Sinibaldi, A. Conti, B. Sinjari, S. Spadone, R. Pecci, M. Palombo, V. S. Komlev, M. G. Ortore, G. Tromba, S. Capuani, R. Guidotti, F. De Luca, S. Caputi, T. Traini, S. Della Penna, *Journal of Tissue Engineering and Regenerative Medicine* **2018**, 12, 750.

Figures

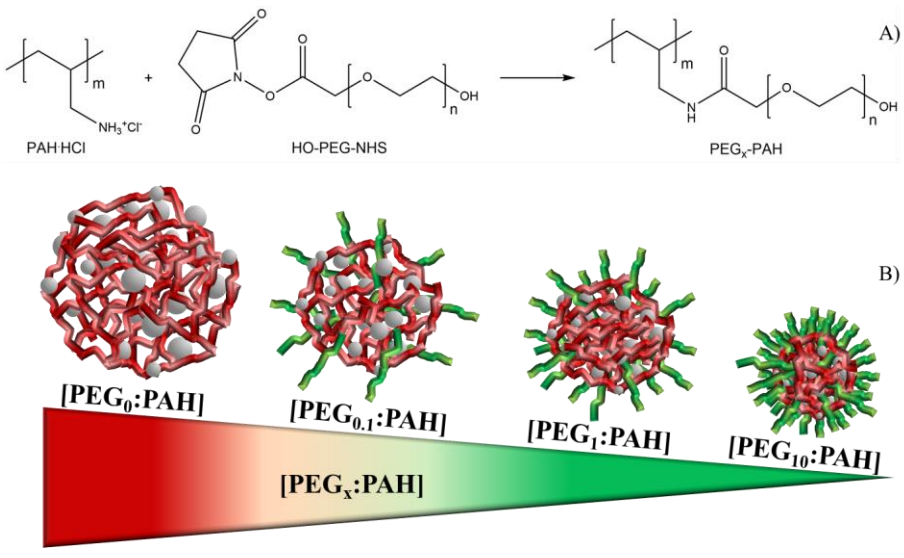

Scheme 1: Synthetic procedure followed for the preparation of the PEGylated PAH NPs.

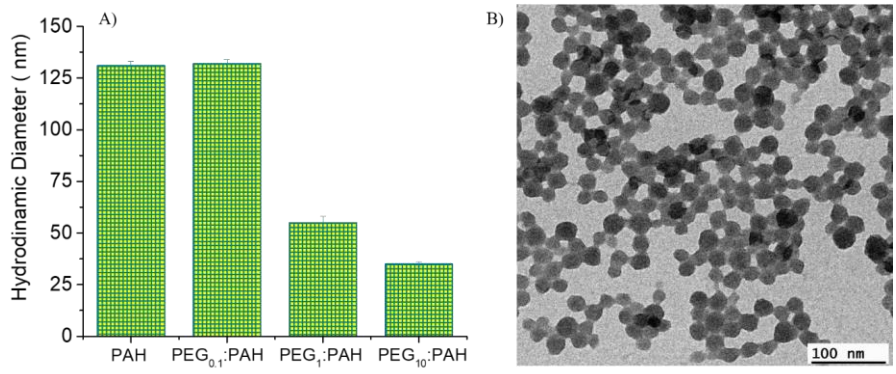

Figure 1: A) Hydrodynamic Diameter obtained by DLS as a function of different molar ratio at 1 mg/mL of PEG_x:PAH (PP) in 5 mM Phosphate Buffer (PB). B) TEM Image of PEGylated PANs obtained with PEG_{10}:PAH ratio in PB 5 mM.

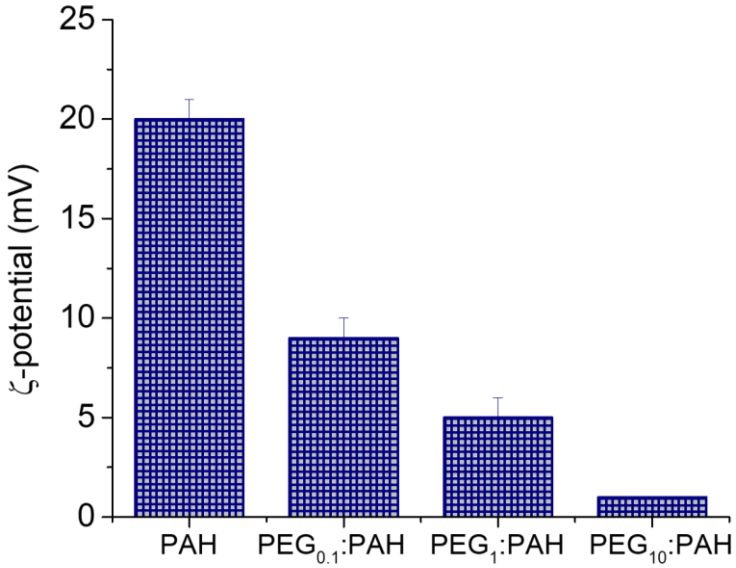

Figure 2: ζ-potential (mV) as a function of different molar ratio at 1 mg/mL of PEG_x:

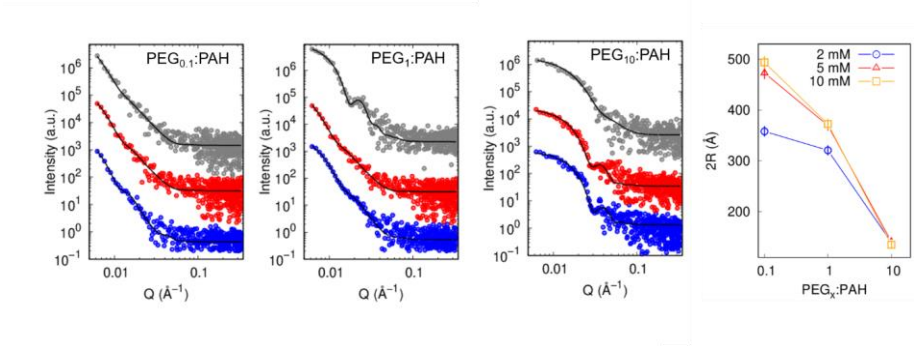

Figure 3: On the left: panel of SAXS experimental curves with their theoretical fitting obtained by GENFIT [F. Spinozzi et al., J Appl Cryst]. SAXS curves (scaled for clarity) in blue, red, and grey indicate respectively PBS concentrations of 2, 5, and 10 mM. The colors in the background indicate the PEG:PAH ratio. The pink, blue and green background indicate PEG:PAH ratios of 0.1 1 and 10, respectively. The fitting curves are reported in black. On the right: PANs average radius as a function of PBS concentration and of PEG:PAH ratio resulting from SAXS data fitting. The legend details the phosphate buffer content. Lines are guide to the eyes.

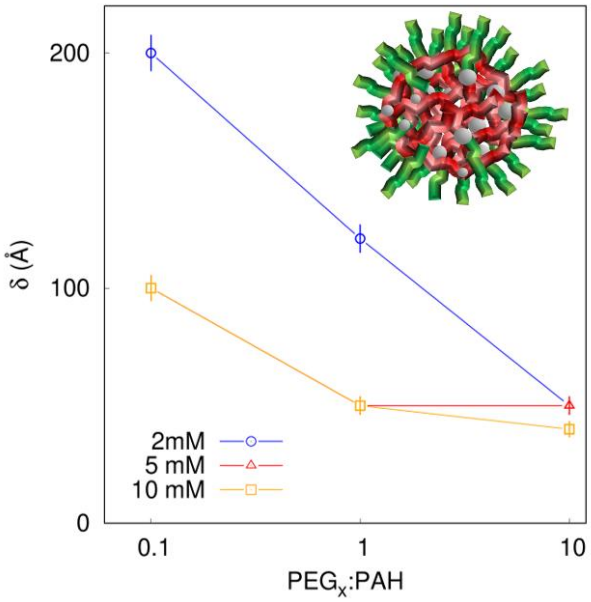

Figure 4: Thickness of PEG shell as a function of PBS content, as reported in the legend, and of PEG:PAH ratio.

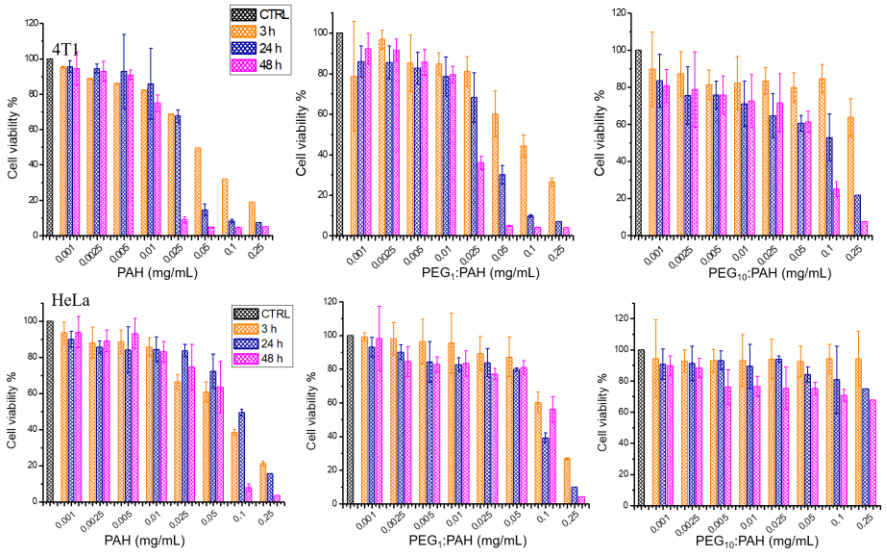

Figure 5. MTT assay for measuring cell proliferation after exposure to PANs and PEGylated PANS for 2 cell lines. Polymer concentration varied from 0.001 to 0.25 mg/mL at different time points, 3, 24 and 48 hours as indicate in the legend. Black bar refers to untreated cells.

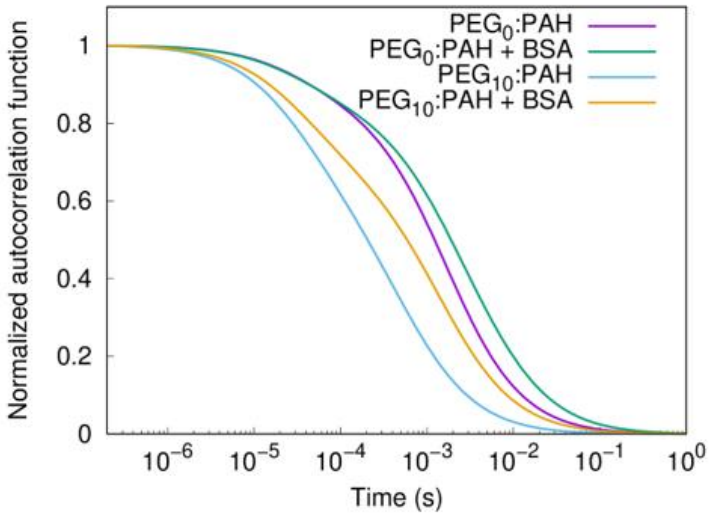

Figure 6. FCS Autocorrelation functions obtained from Fluorescence Correlation Spectroscopy from labelled non-PEGylated PANs (violet, green with BSA) and ~~10~~ PEG_{10}:PAH in PBS (cyan) and in presence of 800 μM BSA in PBS (yellow).

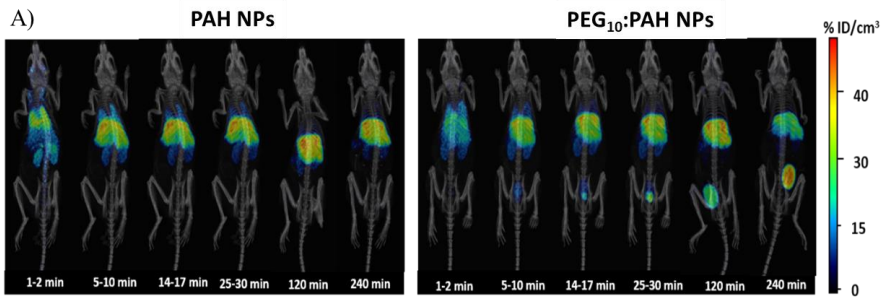

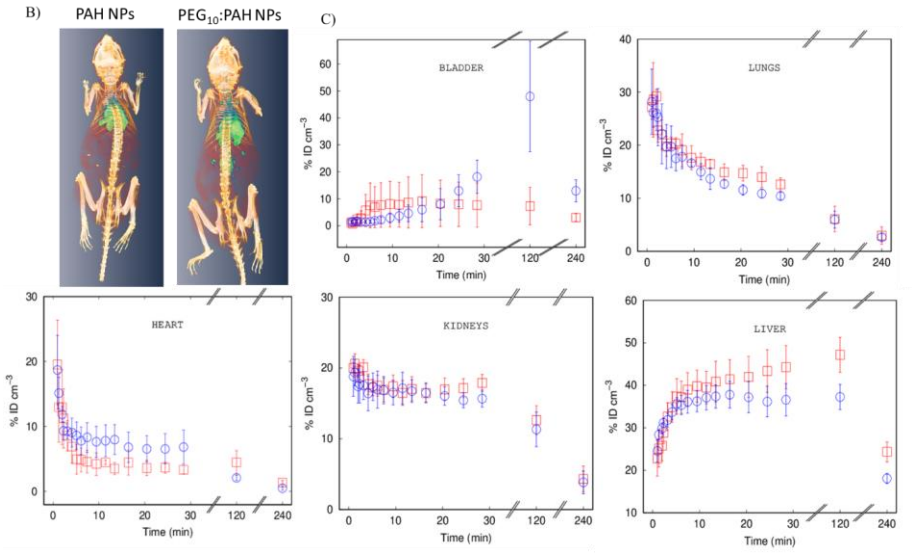

Figure 7. Biodistribution of ^{18}F-PAH/PEG:PAH NPs injected intravenously in female mice; A). Sequence of PET-CT shell images (maximum intensity projections) obtained at different time points; colour regions show activity coming from the nanoparticles. The scale on the left correlates activity intensity with percentage of injected dose per cm^3 (%ID cm^3). B) Three dimensional reconstruction of the PET-CT images ~~for~~ of the biodistribution of non PEGylated PANs and PEG$_{10}$:PAH ~~NPs~~ PANs at 240 min. C) Accumulation of non PEGylated ^{18}F-PAH and ^{18}F-~~/~~PEG:PAH NPs in different organs at different time points, as determined by PET imaging. Results are expressed as % of injected dose per gram. Error bars correspond to the mean ± standard deviation (n=3 per NP type). Green points refer to PEG$_{10}$:PAH ~~NPs~~NPs, violet points to ~~PAH NPs~~non PEGylated NPs.

ha formattato: Apice

ha formattato: Apice

~~**Acknowledgements**~~

~~The authors thank Elettra Synchrotron for beamtime allocation. The authors thank as well the Central European Research Infrastructure Consortium (CERIC) for travel support, and Barbara Sartori for her technical assistance in the chemical laboratory. We thank Multimodal 3D for 3D~~

~~image analysis. We also thank Dr. Richard Murry for correcting the manuscript. S. E. Moya and J. Llop thank the MAT2017-88752-R and CTQ2017-87637-R Retos projects, respectively, from the Ministerio de Economía, Industria y Competitividad, gobierno de España. This work was performed under the Maria de Maeztu Units of Excellence Program from the Spanish State Research Agency – Grant No. MDM-2017-0720.~~

The table of contents entry should be 50–60 words long and should be written in the present tense. The text should be different from the abstract text.

C. Author 2, D. E. F. Author 3, A. B. Corresponding Author* ((same order as byline))

Title ((no stars))

ToC figure ((Please choose one size: 55 mm broad × 50 mm high **or** 110 mm broad × 20 mm high. Please do not use any other dimensions))

((Supporting Information can be included here using this template))

Supporting Information

Title ((no stars))

*Author(s), and Corresponding Author(s)** ((write out full first and last names))

((Please insert your Supporting Information text/figures here. Please note: Supporting Display items, should be referred to as Figure S1, Equation S2, etc., in the main text…)